Research Reports: Biological

Relationships among Bone Quality, Implant Osseointegration, and Wnt Signaling

Journal of Dental Research
2017, Vol. 96(7) 822–831

DOI: 10.1177/0022034517700131
journals.sagepub.com/home/jdr

J. Li[1,2], X. Yin[1,2], L. Huang[2,3], S. Mouraret[2], J.B. Brunski[2], L. Cordova[2,4], B. Salmon[5,6], and J.A. Helms[2]

Abstract

A variety of clinical classification schemes have been proposed as a means to identify sites in the oral cavity where implant osseointegration is likely to be successful. Most schemes are based on structural characteristics of the bone, for example, the relative proportion of densely compact, homogenous (type I) bone versus more trabeculated, cancellous (type III) bone. None of these schemes, however, consider potential biological characteristics of the bone. Here, we employed multiscale analyses to identify and characterize type I and type III bones in murine jaws. We then combined these analytical tools with in vivo models of osteotomy healing and implant osseointegration to determine if one type of bone healed faster and supported osseointegration better than another. Collectively, these studies revealed a strong positive correlation between bone remodeling rates, mitotic activity, and osteotomy site healing in type III bone and high endogenous Wnt signaling. This positive correlation was strengthened by observations showing that the osteoid matrix that is responsible for implant osseointegration originates from Wnt-responsive cells and their progeny. The potential application of this knowledge to clinical practice is discussed, along with a theory unifying the role that biology and mechanics play in implant osseointegration.

Keywords: stem cell, alveolar ridge, osteotomy, bone mineralization, bone density, dental implants

Introduction

Successful implant osseointegration depends on the quality and quantity of interfacial bone, but measuring bone quality is fundamentally difficult (Licata 2009). A variety of clinical classification schemes have been proposed to address this knowledge gap, and most are based on the relative proportion of compact cortical bone to spongy trabecular bone (Lekholm and Zarb 1985; Misch 1989). Type I bone is considered the least vascular and most homogenous, type II is a combination of cortical bone with a marrow cavity, type III is predominantly composed of trabecular bone, and type IV is described as having a very thin cortex and low-density trabeculae (Lekholm and Zarb 1985) and is generally viewed as being unable to support an implant (He et al. 2015). Bone types have been analogized to species of wood ranging from balsa to oak (Greenstein et al. 2010), whereas subsequent classification schemes have codified bone types using quantitative measures (Turkyilmaz et al. 2008). Despite such advances, the diagnostic value of many schemes remains questionable (Ribeiro-Rotta et al. 2007; Ribeiro-Rotta et al. 2011; Lindh et al. 2014).

This, then, was the launching point for our study: to gain insights into why some intraoral sites support osseointegration better than others. We opted to use a mouse model because of the wealth of analytical (molecular, cellular, genetic) tools available. Our first objective was to categorize jaw bones in terms of their microarchitecture, their relative/apparent density, and their level of turnover. Our second objective was to use in vivo models (osteotomy site healing and implant osseointegration) to determine if one type of bone healed faster and supported osseointegration better than another. Collectively, these studies revealed a strong positive correlation between bone remodeling rates, mitotic activity, and osteotomy site

[1]State Key Laboratory of Oral Diseases, West China Hospital of Stomatology, Sichuan University, Chengdu, China
[2]Division of Plastic and Reconstructive Surgery, Department of Surgery, Stanford University School of Medicine, Stanford, CA, USA
[3]Department of Orthodontics, Stomatological Hospital of Chongqing Medical University, Chongqing, China
[4]Department of Oral and Maxillofacial Surgery, School of Dentistry, University of Chile, Santiago, Chile
[5]EA 2496, Orofacial Pathologies, Imaging and Biothérapies Laboratoire, L'Université Paris Descartes, Sorbonne Paris Cité, Montrouge, France
[6]Le Service d'Odontologie de Bretonneau, Hôpitaux Universitaires Paris Nord Val de Seine, Assistance Publique–Hôpitaux de Paris, Paris, France

A supplemental appendix to this article is available online.

Corresponding Author:
J.A. Helms, Division of Plastic and Reconstructive Surgery, Department of Surgery, Stanford University School of Medicine, 1651 Page Mill Drive, Palo Alto, CA 94305, USA.
Email: jhelms@stanford.edu

healing in type III bone and high endogenous Wnt signaling. The potential therapeutic implications of these data are discussed, along with a model integrating the biological data into our current understanding of mechanics and implant osseointegration.

Methods and Materials

Animals in Experimental and Control Groups

Procedures were approved by the Stanford University Committee on Animal Research (#13146) and conformed to ARRIVE guidelines (Kilkenny et al. 2011). Experimental groups are presented in Appendix Table 1. To induce Cre expression in $Axin2^{CreERT2/+}$; $R26R^{mTmG/+}$ mice, a single dose (4 mg/25 mg body weight) of tamoxifen was delivered intraperitoneally 2 d before surgery. The dose and duration of the latency period were verified (Ransom et al. 2016).

There were 4 experimental groups to which animals were randomly assigned (Appendix Table 1). In one group, multiscale analyses were performed on pristine alveolar bone and the edentulous ridge to characterize bone types. In a second group, extraction socket healing was monitored to ensure that the healed site represented type III bone. In a third group, osteotomy healing rates were assessed in type I and type III bones. In the fourth group, implant osseointegration was evaluated as a function of bone type. To minimize animal numbers and control for interanimal variability, a split-mouth design was employed. The experimental unit was bone harvested from the indicated site.

Surgeries

After an appropriate level of anesthesia was reached via an intraperitoneal injection of ketamine/xylazine, maxillary first molars (e.g., M1) were extracted. Bleeding was controlled by local compression. Mice were fed a regular diet and housed in groups of 5. Weight changes were <10%. No adverse events (e.g., uncontrolled pain, infection, prolonged inflammation) were encountered.

After 4 wk, mice were anesthetized, and 2 osteotomies were created using a micro-dissecting trephine. One osteotomy was created using a low-speed (800 rpm) dental engine in the healed M1 extraction site, and another was created in the contralateral edentulous ridge (Appendix Table 1). In a subset of animals, titanium alloy implants (RETOPIN; Edenta) were placed in equivalent osteotomies; again, no adverse events were encountered.

Sample Preparation, Histology, Cellular Assay, and Quantitative Real-Time Polymerase Chain Reaction (qRT-PCR)

Mice were sacrificed on postosteotomy days (PODs) or postimplant days (PIDs) as indicated and prepared for analyses (Appendix Table 2). For qRT-PCR, maxillae were dissected, soft tissues were removed, and a 2-mm biopsy punch was used to collect bone from the edentulous ridge and from a healed extraction site for RNA extraction (Minear et al. 2010). Gene expression levels were determined by the ΔΔCt method and normalized to GAPDH values. Reactions were performed in triplicate, and means ± standard errors were calculated. Primer sequences are presented in Appendix Table 2.

Histomorphometry and Micro–Computed Tomography (μCT) Analyses

Histomorphometric measurements used a minimum of 4 tissue sections to quantify the amount of new bone around the implant (Yin et al. 2015). The percentage of new bone formation was calculated using the ratio of new bone formation/total area of the bone-implant area.

Scans of murine maxillae were completed at a 4-μm resolution (MicroXCT; Xradia). Volumes of interest for microarchitecture analyses focused on the pristine edentulous ridge anterior to M1 and the healed socket. The whole stacked histogram–based threshold BoneJ plugin (Version 1.4.1) was used for automatic binary segmentation of bone (Doube et al. 2010) and to evaluate the bone volume/total volume (BV/TV), trabecular spacing, and trabecular thickness (Bouxsein et al. 2010).

Statistical Analyses

Immunostaining and qRT-PCR were performed by one investigator (J.L.) and quantifications by others (X.Y., L.H.). Results are presented as the mean ± standard error of independent replicates. The Student's t test was used to quantify differences described in this article. $P \leq 0.05$ was considered significant.

Results

Multiscale Analyses of Murine Bone Types

Clinical descriptions (Lekholm and Zarb 1985; Misch 1989) were used to identify potential type I and type III bones. To avoid the introduction of possible bias based on an embryonic origin (Leucht et al. 2008), and because we were primarily interested in dental implants, we focused solely on jaw bones. The murine maxillary edentulous ridge is composed of compact lamellar bone, and the adjacent maxilla is composed of alveolar bone with marrow cavities (Fig. 1A, B). The BV/TV is significantly higher in the edentulous ridge compared to alveolar bone (Fig. 1C). Accordingly, the maxillary edentulous ridge was characteristic of type I bone, and the adjacent alveolar bone was characteristic of type III bone.

We evaluated the 2 bone types further: The osteocyte number/mineralized matrix volume was not significantly different, but osteocyte organization and morphology were. Osteocytes in type I bone were spindle-shaped and had parallel organization versus osteocytes in type III bone, which had a rounded morphology (Fig. 1D–F, Appendix Fig. 1A). Collagen fiber organization is dictated in part by osteocytes (Kerschnitzki et al. 2011), and using Picrosirius red staining, the arrangement of

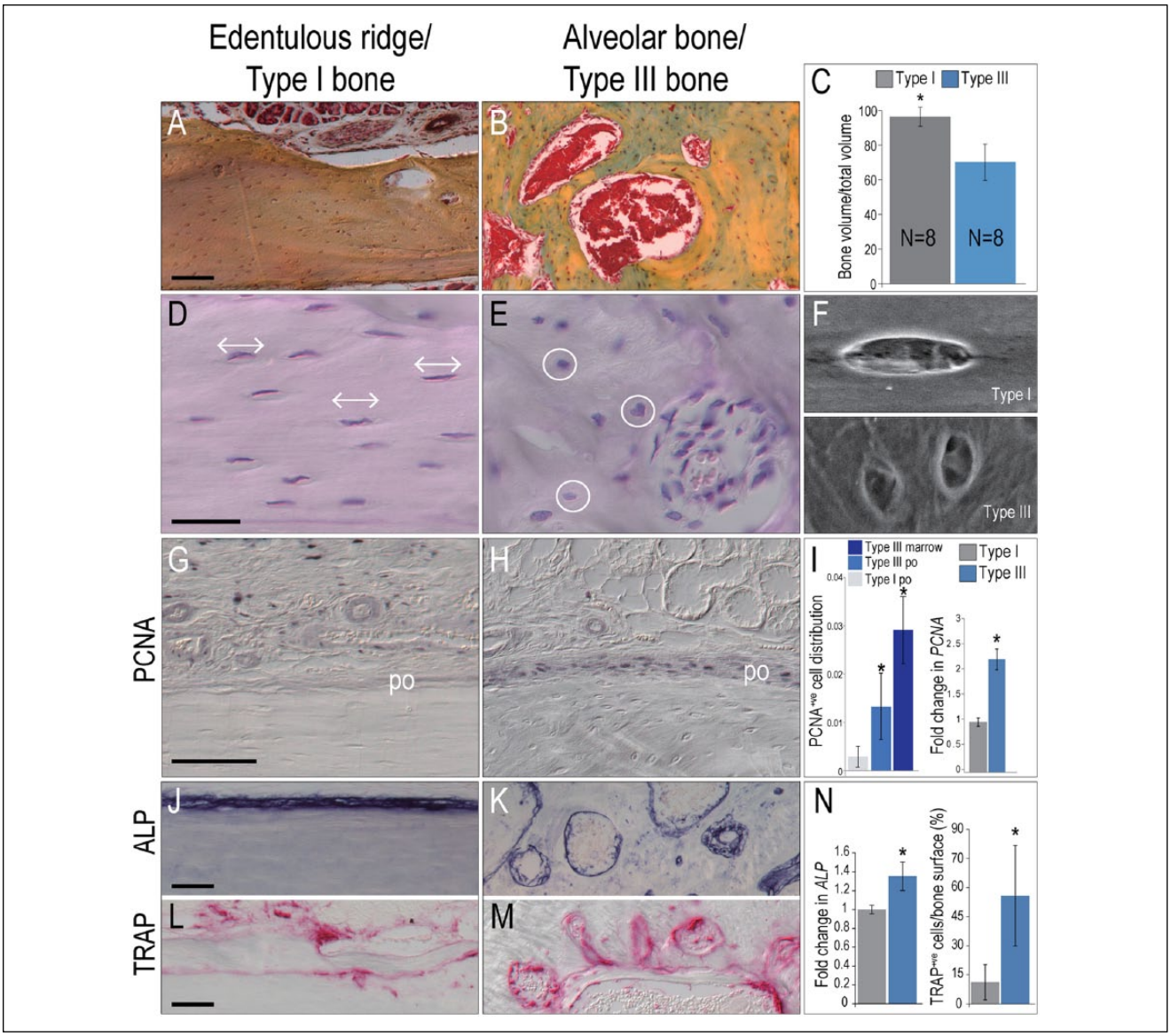

Figure 1. Multiscale analyses of craniofacial bones identify type I and type III bones in the mouse maxilla. Representative sagittal tissue sections stained with Movat pentachrome from the (**A**) edentulous ridge (e.g., type I bone) and (**B**) alveolar bone between M1 and M2 (e.g., type III bone). (**C**) Quantification of micro–computed tomography data, demonstrating that type I bone has a significantly higher bone volume/total volume than type III bone. Representative tissue sections stained with hematoxylin and eosin show (**D**) flattened, elongated osteocytes (arrows) in type I bone and (**E**) osteocytes with a rounded morphology (circles) in type III bone. (**F**) Scanning electron microscopy of lacunae in type I and type III bone. Immunostaining for proliferating cell nuclear antigen (PCNA) in the periosteum of (**G**) type I and (**H**) type III bone. (**I**) Quantification of PCNA cell distribution in the marrow and periosteum of type I and type III bone, and quantitative real-time polymerase chain reaction of PCNA expression in type I and type III bone. Alkaline phosphatase (ALP) activity in (**J**) the periosteum of type I bone and (**K**) on endosteal surfaces of vascular lacunae in type III bone. Tartrate-resistant acid phosphatase (TRAP) activity in (**L**) the periosteum of type I bone and (**M**) on endosteal surfaces of vascular lacunae in type III bone. (**N**) Quantification of ALP expression in type I and type III bones, and quantification of the number of $TRAP^{+ve}$ cells, expressed as a percentage of the bone surface examined. po, periosteum. Asterisk indicates $P < 0.05$. Scale bars = 50 μm for all panels.

collagen fibers was visualized. In type I bone, collagen fibers were homogenous, densely packed, and linearly arranged, while in type III bone, the fibers had a basketweave pattern (Appendix Fig. 1B, C). Osteocyte density was equivalent between the 2 types of bone (Appendix Fig. 1D, E).

Mitotic activity is often used as an indicator of the healing potential (Jacobsson et al. 1985; Yang et al. 2015). Immunostaining for proliferating cell nuclear antigen (PCNA) revealed few mitotically active cells in the periosteum of type I bone but an abundance of proliferating cells in the periosteum and marrow spaces of type III bone (Fig. 1G, H, Appendix Fig. 1G). Our inability to detect $PCNA^{+ve}$ cells in type I periosteum was not due to technical difficulties because in the same tissue section, $PCNA^{+ve}$ cells were abundant in the adjacent gingiva (Appendix Fig. 1F). This distribution of mitotically active cells was confirmed using a second molecular marker, Ki67 (Appendix Fig.

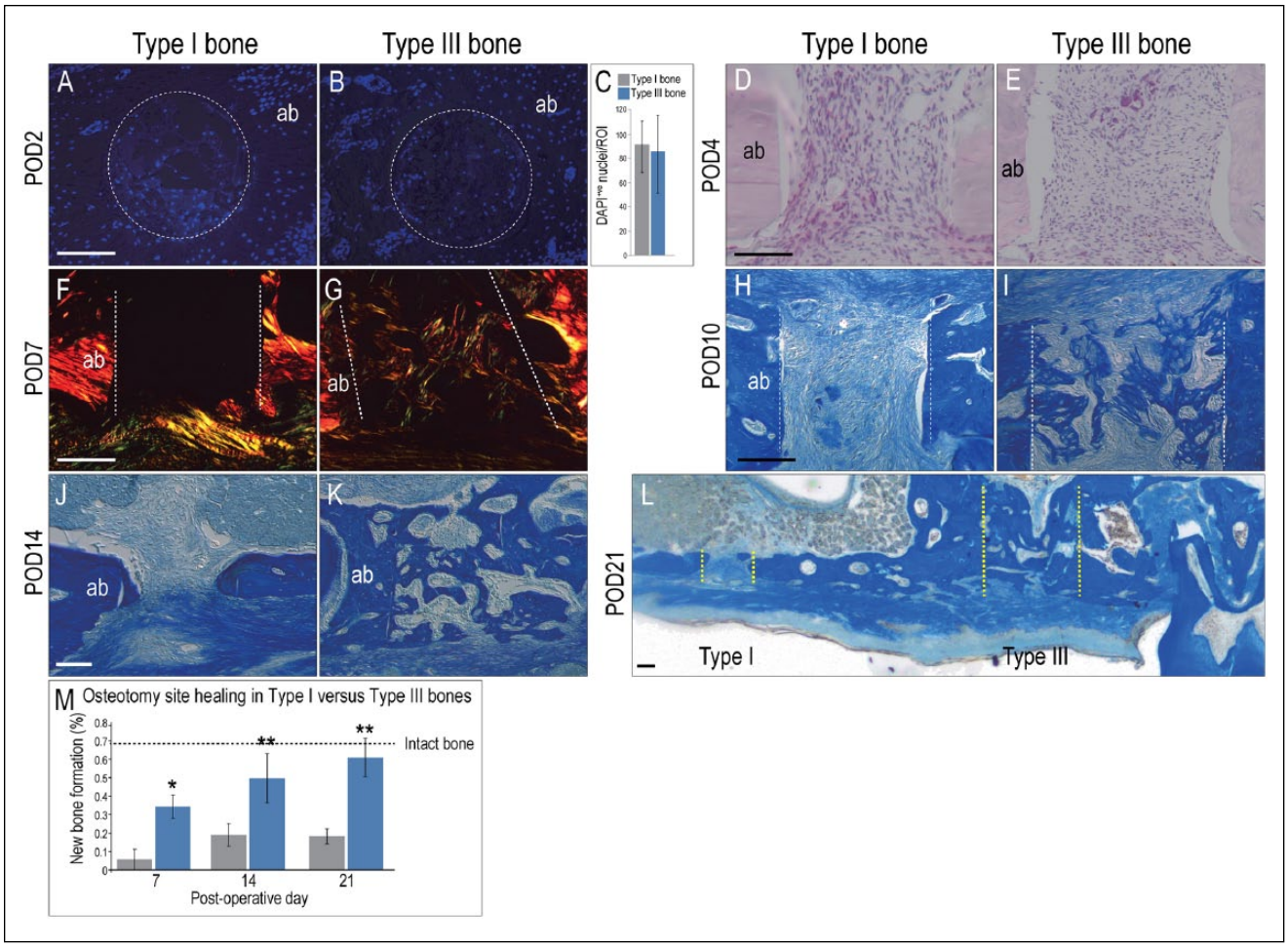

Figure 2. Osteotomy healing is significantly faster in type III bones. On postosteotomy day 2 (POD2), representative transverse tissue sections were stained with DAPI to assess cell density in osteotomy sites created in (**A**) type I and (**B**) type III bones; (**C**) quantification of cell density within a specified region of interest. Sagittal tissue sections from POD4, stained with hematoxylin and eosin to visualize cell density in osteotomies created in (**D**) type I and (**E**) type III bones. Sagittal tissue sections from POD7, stained with Picrosirius red and then viewed under polarized light to visualize collagen deposition in osteotomies created in (**F**) type I and (**G**) type III bone. Dotted white lines indicate osteotomy edges. Aniline blue staining identifies a new osteoid matrix in osteotomies created in (**H**) type I and (**I**) type III bones on POD10 and (**J**, **K**) POD14. (**L**) On POD21, the osteotomy in type I bone is still in the process of repair, whereas the osteotomy site in type III bone is healed; yellow dotted lines mark osteotomy edges. (**M**) Quantification of Aniline blue^{+ve} pixels in osteotomy sites at time points indicated. Dotted black line indicates the percentage of Aniline blue^{+ve} pixels observed in the same volume of intact alveolar bone. ab, alveolar bone. Asterisk indicates $P < 0.05$. Scale bar = 50 μm for all panels.

1H, I). qRT-PCR verified that *PCNA* expression was elevated in type III bone (Fig. 1I).

Rapid bone remodeling is regarded as a hallmark of the healing potential (Hernandez and Keaveny 2006); therefore, we evaluated the distribution of osteoblast and osteoclast activities (Appendix Table 2). In both types of bone, nearly all periosteal and endosteal surfaces stained positive for alkaline phosphatase (ALP) (Fig. 1J, K, Appendix Fig. 1J, K), but type III bone had significantly more tartrate-resistant acid phosphatase (TRAP^{+ve}) osteoclasts (Fig. 1L, M), and both ALP and TRAP were expressed at significantly higher levels in type III bone (Fig. 1N). Type III bone is differentiated from type I bone by the presence of marrow spaces (Fig. 1A, B), and accordingly, we detected more CD31^{+ve} endothelial cells in type III bone (Appendix Fig. 1L, M). Taken together, we concluded that type III bone had a higher mitotic index and was turning over faster than type I bone.

Type I and Type III Bones Have Different Healing Potentials

An osteotomy model was used to ascertain the healing potential of type I and type III bones. To create a large enough space for implant insertion, the maxillary first molars were extracted and the sockets allowed to heal completely (Appendix Fig. 2A–D). Histomorphometric analyses confirmed that the BV/TV of the healed site was equivalent to intact type III bone (Appendix Fig. 2E, F). Contralateral osteotomies were then generated in the healed extraction socket and the edentulous ridge.

Early during healing (e.g., POD2 and POD4), type I and type III bones appeared equivalent in terms of the density of cells occupying the osteotomies (Fig. 2A–E), but by POD7, the first differences were detectable. Osteotomies in type III bone were filled with a mineralizing collagen matrix, whereas no new collagen was evident in osteotomies in type I bone (Fig. 2F, G). The rate of new bone formation was significantly faster in type III bone osteotomies compared to equivalent osteotomies in type I bone (Fig. 2H–L; histomorphometric quantification in Fig. 2M).

Implants Osseointegrate More Efficiently in Type III Bone

We reasoned that if new bone formed more rapidly in type III bone osteotomies, then implants placed in these osteotomies should also osseointegrate faster. To minimize discrepancies in healing rates related to anatomic location, the 2 implant sites were separated by approximately 2 mm but were performed contralaterally so that one implant bed did not impinge on the other (Appendix Fig. 2G). Implants were placed into slightly oversized osteotomies (Yin et al. 2016) (Appendix Table 1), which resulted in a 25 μm–wide circumferential gap interface around the implants (yellow asterisk in Fig. 3A). This challenging scenario allowed us to compare healing responses between the 2 bone types. Visual inspection confirmed that implants were placed to the same depth, below the level of the occlusal plane. None of the implants were intentionally loaded.

Initially, the interfacial gaps in both types of bone were occupied by a fibrin-rich extracellular matrix and cells (Fig. 3B, C); the difference was that in type I bone, cells expressed the fibrotic marker vimentin (Fig. 3D) and weakly expressed the osteoprogenitor marker Runx2 (Fig. 3E). In type III bone, the opposite was true: cells in the gap showed weak vimentin (Fig. 3F) and strong Runx2 (Fig. 3G) expression. By PID7, differences in proliferation and mineralization were also evident. Implants placed in type I bone had few proliferating cells and no mineralization (Fig. 3H, I), whereas implants placed in type III bone were surrounded by proliferating cells and a mineralizing extracellular matrix (Fig. 3J, K, Appendix Fig. 2H, I). By PID14, implants placed in type I bone were encapsulated by a fibrous envelope (Fig. 3L), whereas implants placed in type III bone were encased in bone (Fig. 3M).

Wnt-Responsive Cells Are Responsible for Implant Osseointegration

To gain insights into the molecular basis for the superior bone-forming ability in type III bone, we assessed endogenous Wnt signaling using the *Axin2*$^{LacZ/+}$ strain of mice (Lustig et al. 2002) in which Wnt-responsive populations are Xgal^{+ve} (Fig. 4A). Xgal^{+ve} cells were largely absent from type I bone (Fig. 4B) but were abundant in both the periosteum and marrow spaces of type III bone (Fig. 4C). qRT-PCR verified that *Axin2* was expressed at significantly higher levels in type III bone (Fig. 4D). The same observation was made during osteotomy site healing: type I bone osteotomies were devoid of Xgal^{+ve} cells, while type III bone osteotomies were filled with Xgal^{+ve} cells (Fig. 4E, F, Appendix Fig. 2J–M).

These data indicated a positive correlation between endogenous Wnt responsiveness and a bone's osteogenic properties. To demonstrate a causal link between Wnt signaling and osteogenesis, we used a lineage-tracing strain, *Axin2*$^{CreErt2/+}$*; R26*$^{mTmG/+}$ (van Amerongen et al. 2012), in which *Axin2*$^{+ve}$ Wnt-responsive cells and their progeny express green fluorescent protein (GFP) (Fig. 4G). This lineage tracer permitted us to follow the fates of the Wnt-responsive cells and determine if those cells ultimately gave rise to bone around the implant.

We first confirmed that the initial distribution of GFP^{+ve} Wnt-responsive cells was similar to the distribution of Xgal^{+ve} Wnt-responsive cells (Fig. 4H, I, Appendix Fig. 3A–D) and then used Runx2 co-immunostaining to demonstrate that most Wnt-responsive progeny were osteoprogenitors (Fig. 4J). Oversized osteotomies were then generated in type I and type III bones of the *Axin2*$^{CreErt2/+}$*; R26*$^{mTmG/+}$ reporter, implants were placed, and peri-implant tissues were analyzed over the next 4 wk.

In type I bone, GFP immunostaining was nearly undetectable (Appendix Fig. 3E, F), and as before, implants failed to osseointegrate (Fig. 3). In contrast, GFP immunostaining was abundant around implants placed in type III bone (Fig. 4K). By PID14, when the implants were osseointegrated, we found that the peri-implant bone was primarily composed of GFP^{+ve}, Runx2^{+ve} osteoblasts (Fig. 4L, M). Thus, most of the new bone that supported the implants in type III bone arose from Wnt-responsive cells. Collectively, these data establish a causal link between endogenous Wnt signaling, the regenerative potential of bones in the oral cavity, and osseointegration.

Discussion

Anatomic Predictors of Implant Success

Predicting implant success is an inherently difficult challenge. Surgeon skill, patient health, implant design and manufacture, osteotomy site preparation, and mechanical loading all contribute to the success or failure of dental implants. Some investigators also consider anatomic location as a key variable (Jaffin and Berman 1991; He et al. 2015), while others claim it is not (Glauser et al. 2005; Cochran et al. 2009; Kim et al. 2011). Unfortunately, our study cannot shed light on whether anatomic location influences implant success because anatomic location is not synonymous with bone type. While it is true that in older patients the anterior atrophic mandible is predominantly type I bone and the posterior maxilla is type III bone (Adell et al. 1981; Monje et al. 2015), it is also the case that human jaw bones show extreme variation in density, even within the same anatomic site (Ulm et al. 1999; Monje et al. 2015). Consequently, reports on clinical implant success as a function of anatomic location cannot be directly compared with our study in which implant osseointegration is correlated

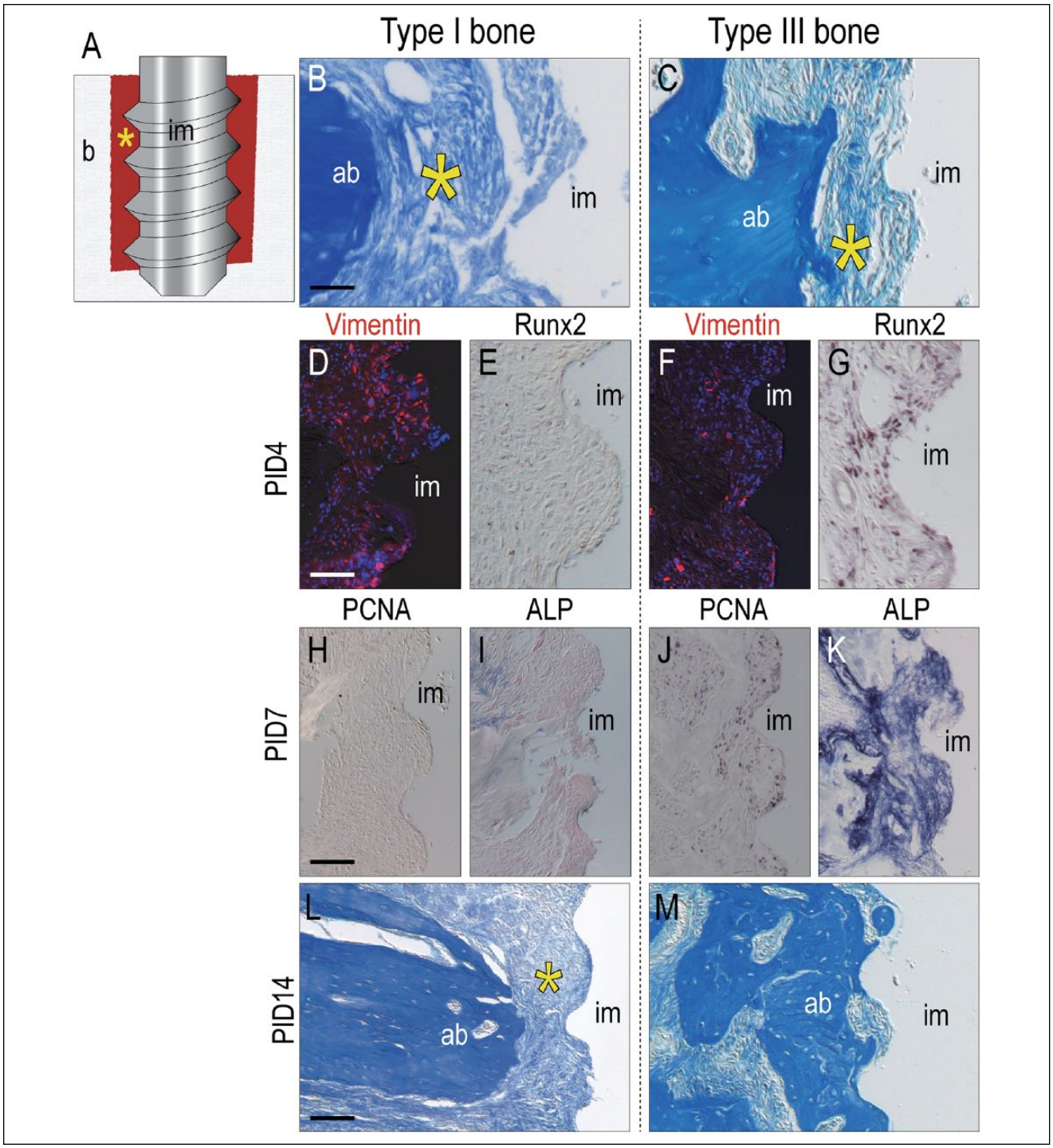

Figure 3. The regenerative capacity of type III bone is greater than type I bone, which results in faster implant osseointegration. (**A**) Schematic of the gap-interface model employed, where the external diameter of the implant is smaller than the diameter of the osteotomy. Yellow asterisk marks the gap interface. Representative tissue sections stained with Aniline blue show the gap interface (yellow asterisk) around implants placed in (**B**) type I and (**C**) type III bones. On postimplant day 14 (PID4), immunostaining for (**D**) the fibrogenic marker vimentin and (**E**) the osteogenic marker Runx2 in interfacial tissues of type I bone. (**F**) Vimentin and (**G**) Runx2 immunostaining in interfacial tissues of type III bone. On PID7, immunostaining for (**H**) proliferating cell nuclear antigen (PCNA) and (**I**) alkaline phosphatase (ALP) activity in interfacial tissues of type I bone. (**J**) PCNA and (**K**) ALP activity in interfacial tissues of type III bone. (**L**) On PID14, the gap interface persists around implants in type I bone, whereas (**M**) implants have osseointegrated in type III bone. ab, alveolar bone; im, implant. Scale bars = 50 µm for all panels.

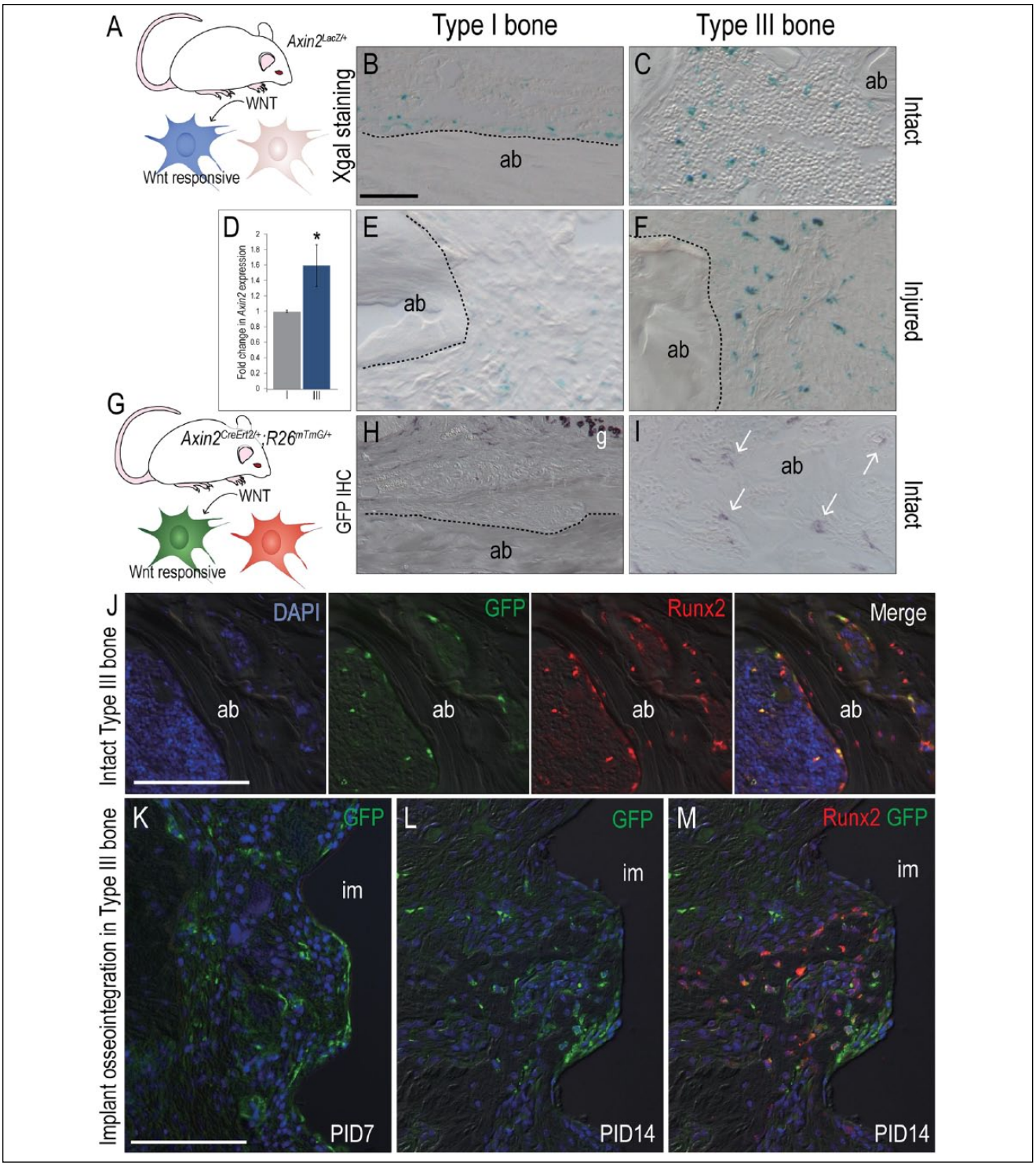

Figure 4. The Wnt-responsive status of a bone correlates with the bone-forming potential. (**A**) Schematic of the Axin2$^{LacZ/+}$ strain, where positive Xgal staining identifies Wnt-responsive cells. Xgal staining shows (**B**) a paucity of Wnt-responsive cells in intact type I bone compared to (**C**) the relative abundance of Xgal^{+ve} cells in type III vascular lacunae. (**D**) Quantitative real-time polymerase chain reaction for Axin2 mRNA in type I versus type III bone. Xgal staining shows (**E**) few Wnt-responsive cells in osteotomies created in type I bone compared to (**F**) many Xgal^{+ve} cells in osteotomies created in type III bone. (**G**) Schematic of the Axin2$^{CreERT2/+}$; R26R$^{mTmG/+}$ strain, where green fluorescent protein (GFP) immunostaining identifies Wnt-responsive cells and their progeny. Also, 7 d after a tamoxifen injection, GFP immunostaining identifies (**H**) no Wnt-responsive progeny in intact type I bones but (**I**) many Wnt-responsive progeny in the vascular lacunae of intact type III bones. (**J**) Co-immunostaining of GFP and Runx2 shows that most Wnt-responsive progeny are osteoprogenitor cells. (**K**) Peri-implant tissues on postimplant day 7 (PID7) are primarily composed of Wnt-responsive progeny. (**L**) On PID14, the Wnt-responsive progeny (**M**) co-express Runx2, demonstrating that peri-implant bone arose from a Wnt-responsive population. ab, alveolar bone; im, implant. Scale bar = 50 μm for all panels.

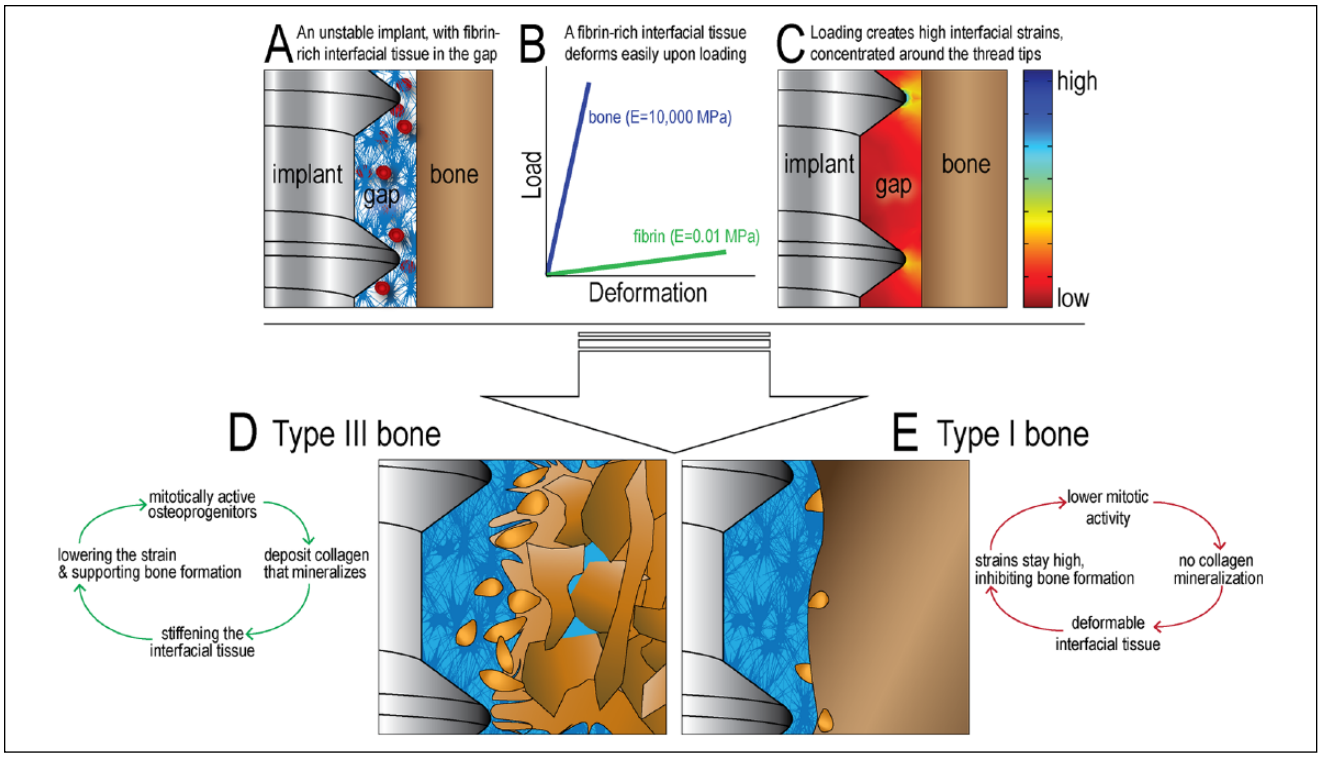

Figure 5. The Wnt-responsive status of a bone correlates with the bone-forming potential. (**A**) Schematic of the Axin2$^{LacZ/+}$ strain, where positive Xgal staining identifies Wnt-responsive cells. Xgal staining shows (**B**) a paucity of Wnt-responsive cells in intact type I bone compared to (**C**) the relative abundance of Xgal^{+ve} cells in type III vascular lacunae. (**D**) Quantitative real-time polymerase chain reaction for Axin2 mRNA in type I versus type III bone. Xgal staining shows (**E**) few Wnt-responsive cells in osteotomies created in type I bone compared to (**F**) many Xgal^{+ve} cells in osteotomies created in type III bone. (**G**) Schematic of the Axin2$^{CreERT2/+}$; R26R$^{mTmG/+}$ strain, where green fluorescent protein (GFP) immunostaining identifies Wnt-responsive cells and their progeny. Also, 7 d after a tamoxifen injection, GFP immunostaining identifies (**H**) no Wnt-responsive progeny in intact type I bones but (**I**) many Wnt-responsive progeny in the vascular lacunae of intact type III bones. (**J**) Co-immunostaining of GFP and Runx2 shows that most Wnt-responsive progeny are osteoprogenitor cells. (**K**) Peri-implant tissues on postimplant day 7 (PID7) are primarily composed of Wnt-responsive progeny. (**L**) On PID14, the Wnt-responsive progeny (**M**) co-express Runx2, demonstrating that peri-implant bone arose from a Wnt-responsive population. ab, alveolar bone; im, implant. Scale bar = 50 µm for all panels.

with bone type. In the following paragraphs, we address this knowledge gap and focus on how observations made in this study may be translated into clinically useful information.

Biological Predictors of Implant Success

Clinical classification schemes are largely based on the structural characteristics of bone rather than their biological characteristics. Therefore, our first objective was to identify type I and type III bones in the murine oral cavity and then use multiscale analyses to determine if rodents, like humans (Buser et al. 2004), had bones that differed in their regenerative potential.

Three biological characteristics emerged that distinguished murine type I bone from type III bone. First, there were significantly more proliferating cells in the periosteum of type III bone than in type I bone (Fig. 1). This was actually anticipated from previous experiments, where the periosteums of alveolar and long bones were compared (Mouraret et al. 2014). Second, relative to type I bone, type III bone exhibited significantly more remodeling activity (Fig. 1). A growing literature emphasizes the link between tissue remodeling, healing potential, and the presence of stem cell pools (Eming et al. 2014), and in keeping with this association, we uncovered a third biological difference: type III bone had significantly more Wnt stem/osteoprogenitor cells, and a significantly higher expression of Wnt target genes, than type I bone (Fig. 3).

Higher Wnt signaling correlates with faster osteotomy healing and faster implant osseointegration (Fig. 4), but that does not mean that there is a causal link between the variables. That link was established in a previous study in which the delivery of WNT3A protein induced osseointegration (Yin et al. 2015). Even though the implants lacked primary stability, adding exogenous WNT3A was sufficient to transform a fibrous, encapsulated implant to an osseointegrated one (Yin et al. 2015). Coupling those data with observations made in this study, we suggest that a WNT protein therapeutic may be a viable strategy to ensuring osseointegration of implants, even if they are placed into sites with a low regenerative potential.

A Unifying Theory for Mechanobiological Predictors of Implant Success

We integrate these biological findings into our understanding of mechanics and implant osseointegration. We begin with the

knowledge that all dental implants are subjected to loading, whether it be an incidental, nominal load placed on a submerged implant or an intentional masticatory load placed on an immediate implant. In either case, loading creates strain in the tissues surrounding the implant (Leucht et al. 2007), and the magnitude of that strain depends on 2 factors: the load vector (i.e., its magnitude and direction) and the properties of the interfacial tissues. Experiments undertaken here set the stage for understanding how those interfacial tissues differ depending on the type of bone into which the implant is placed.

By creating oversized osteotomies in both types of bone, we ensured that our implants were surrounded by a pliable fibrin clot and were therefore unstable (Yin et al. 2015) (Fig. 5A). A fibrin clot has a very low elastic modulus; that is, it is easily deformed by loading (Fig. 5B). Consequently, even minimal incidental loading of a partially submerged implant will create high strain at the tips of the implant threads; between the threads, however, the strains are much lower (Yin et al. 2015) (Fig. 5C). The distribution of these high and low strains in the pliable fibrin clot provided clues as to what likely transpires around a healing implant.

In bones with a greater regenerative potential (e.g., type III bones), cells in the low-strain region proliferate and deposit a collagen matrix, and the collagen matrix begins to mineralize (Fig. 4, schematized in Fig. 5D). The presence of a mineralizing matrix stiffens the interfacial environment, which lowers the strain and thus favors bone formation (Carter and Beaupre 2001). This positive feedback loop exists in type III bone and ultimately manifests as implant osseointegration (Fig. 4). What about type I bone (Fig. 5E)? Here, a lower rate of cell proliferation, coupled with minimal collagen deposition and no mineralization, means that the interfacial tissues fail to stiffen, and strains remain high (Yin et al. 2015). This high-strain environment favors the formation of fibrous tissue (Carter and Beaupre 2001). In our experiments this negative feedback loop manifested as fibrous encapsulation of the implant (Fig. 4).

Ultimately, our objective is to translate these basic science observations into actual clinical practice, and these data provide 2 strategies towards achieving that goal. First, we can develop methods to enhance the regenerative potential of an osteotomy site by careful osteotomy site preparation and perhaps by activating skeletal stem cells to hasten bone formation (Leucht et al. 2013). Second, we can develop new implants whose design inherently reduces interfacial strains and thus favors the formation of bone. Both strategies represent novel methods to improve and extend the use of implants in the oral cavity.

Author Contributions

J. Li, contributed to data acquisition, analysis, and interpretation, drafted the manuscript; X. Yin, L. Huang, L. Cordova, contributed to data acquisition, analysis, and interpretation, critically revised the manuscript; S. Mouraret, B. Salmon, contributed to conception and design, critically revised the manuscript; J.B. Brunski, contributed to data analysis and interpretation, critically revised the manuscript; J.A. Helms, contributed to conception, design, data analysis, and interpretation, drafted and critically revised the manuscript. All authors gave final approval and agree to be accountable for all aspects of the work.

Acknowledgments

This work was supported by National Institutes of Health grant 5 R01 DE024000-12 to J.A.H. and J.B.B., National Natural Science Foundation of China grants to J.L. (81500829) and L.H. (81300914), and the University of Chile–Conicyt Becas Chile Award (CONICYT PAI/INDUSTRIA 79090016) to L.C. The authors declare no potential conflicts of interest with respect to the authorship and/or publication of this article.

References

Adell R, Lekholm U, Rockler B, Brånemark PI. 1981. A 15-year study of osseointegrated implants in the treatment of the edentulous jaw. Int J Oral Surg. 10(6):387–416.

Bouxsein ML, Boyd SK, Christiansen BA, Guldberg RE, Jepsen KJ, Muller R. 2010. Guidelines for assessment of bone microstructure in rodents using micro-computed tomography. J Bone Miner Res. 25(7):1468–1486.

Buser D, Martin W, Belser UC. 2004. Optimizing esthetics for implant restorations in the anterior maxilla: anatomic and surgical considerations. Int J Oral Maxillofac Implants. 19 Suppl:43–61.

Carter DR, Beaupre GS. 2001. Skeletal function and form. Cambridge: Cambridge University Press.

Cochran DL, Schou S, Heitz-Mayfield LJ, Bornstein MM, Salvi GE, Martin WC. 2009. Consensus statements and recommended clinical procedures regarding risk factors in implant therapy. Int J Oral Maxillofac Implants. 24 Suppl:86–89.

Doube M, Klosowski MM, Arganda-Carreras I, Cordelières FP, Dougherty RP, Jackson JS, Schmid B, Hutchinson JR, Shefelbine SJ. 2010. BoneJ: free and extensible bone image analysis in ImageJ. Bone. 47(6):1076–1079.

Eming SA, Martin P, Tomic-Canic M. 2014. Wound repair and regeneration: mechanisms, signaling, and translation. Sci Transl Med. 6(265):265sr6.

Glauser R, Ruhstaller P, Windisch S, Zembic A, Lundgren A, Gottlow J, Hammerle CH. 2005. Immediate occlusal loading of branemark system tiunite implants placed predominantly in soft bone: 4-year results of a prospective clinical study. Clin Implant Dent Relat Res. 7 Suppl 1:S52–S59.

Greenstein G, Cavallaro J, Greenstein B, Tarnow D. 2010. Treatment planning implant dentistry with a 2-mm twist drill. Compend Contin Educ Dent. 31(2):126–128, 130, 132 passim; quiz 137–138.

He J, Zhao B, Deng C, Shang D, Zhang C. 2015. Assessment of implant cumulative survival rates in sites with different bone density and related prognostic factors: an 8-year retrospective study of 2,684 implants. Int J Oral Maxillofac Implants. 30(2):360–371.

Hernandez CJ, Keaveny TM. 2006. A biomechanical perspective on bone quality. Bone. 39(6):1173–1181.

Jacobsson M, Albrektsson T, Turesson I. 1985. Dynamics of irradiation injury to bone tissue: a vital microscopic investigation. Acta Radiol Oncol. 24(4):343–350.

Jaffin RA, Berman CL. 1991. The excessive loss of branemark fixtures in type iv bone: a 5-year analysis. J Periodontol. 62(1):2–4.

Kerschnitzki M, Wagermaier W, Roschger P, Seto J, Shahar R, Duda GN, Mundlos S, Fratzl P. 2011. The organization of the osteocyte network mirrors the extracellular matrix orientation in bone. J Struct Biol. 173(2):303–311.

Kilkenny C, Browne W, Cuthill IC, Emerson M, Altman DG; National Centre for the Replacement, Refinement and Reduction of Animals in Research. 2011. Animal research: reporting in vivo experiments. The ARRIVE guidelines. J Cereb Blood Flow Metab. 31(4):991–993.

Kim JS, Sohn JY, Park JC, Jung UW, Kim CS, Lee JH, Shim JS, Lee KW, Choi SH. 2011. Cumulative survival rate of astra tech implants: a retrospective analysis. J Periodontal Implant Sci. 41(2):86–91.

Lekholm U, Zarb G. 1985. Patient selection and preparation. Chicago: Quintessence.

Leucht P, Jiang J, Cheng D, Liu B, Dhamdhere G, Fang MY, Monica SD, Urena JJ, Cole W, Smith LR, et al. 2013. Wnt3a reestablishes osteogenic capacity to bone grafts from aged animals. J Bone Joint Surg Am. 95(14):1278–1288.

Leucht P, Kim JB, Amasha R, James AW, Girod S, Helms JA. 2008. Embryonic origin and hox status determine progenitor cell fate during adult bone regeneration. Development. 135(17):2845–2854.

Leucht P, Kim JB, Wazen R, Currey JA, Nanci A, Brunski JB, Helms JA. 2007. Effect of mechanical stimuli on skeletal regeneration around implants. Bone. 40(4):919–930.

Licata A. 2009. Bone density vs bone quality: what's a clinician to do? Cleve Clin J Med. 76(6):331–336.

Lindh C, Oliveira GH, Leles CR, do Carmo Matias Freire M, Ribeiro-Rotta RF. 2014. Bone quality assessment in routine dental implant treatment among Brazilian and Swedish specialists. Clin Oral Implants Res. 25(9):1004–1009.

Lustig B, Jerchow B, Sachs M, Weiler S, Pietsch T, Karsten U, van de Wetering M, Clevers H, Schlag PM, Birchmeier W, et al. 2002. Negative feedback loop of wnt signaling through upregulation of conductin/axin2 in colorectal and liver tumors. Mol Cell Biol. 22(4):1184–1193.

Minear S, Leucht P, Jiang J, Liu B, Zeng A, Fuerer C, Nusse R, Helms JA. 2010. Wnt proteins promote bone regeneration. Sci Transl Med. 2(29):29ra30.

Misch CE. 1989. Bone classification, training keys to implant success. Dent Today. 8(4):39–44.

Monje A, Gonzalez-Garcia R, Monje F, Chan HL, Galindo-Moreno P, Suarez F, Wang HL. 2015. Microarchitectural pattern of pristine maxillary bone. Int J Oral Maxillofac Implants. 30(1):125–132.

Mouraret S, Von Kaeppler E, Bardet C, Hunter DJ, Chaussain C, Bouchard P, Helms JA. 2014. The potential for vertical bone regeneration via maxillary periosteal elevation. J Clin Periodontol. 41(12):1170–1177.

Ransom RC, Hunter DJ, Hyman S, Singh G, Ransom SC, Shen EZ, Perez KC, Gillette M, Li J, Liu B, et al. 2016. Axin2-expressing cells execute regeneration after skeletal injury. Sci Rep. 6:36524.

Ribeiro-Rotta RF, Lindh C, Pereira AC, Rohlin M. 2011. Ambiguity in bone tissue characteristics as presented in studies on dental implant planning and placement: a systematic review. Clin Oral Implants Res. 22(8):789–801.

Ribeiro-Rotta RF, Lindh C, Rohlin M. 2007. Efficacy of clinical methods to assess jawbone tissue prior to and during endosseous dental implant placement: a systematic literature review. Int J Oral Maxillofac Implants. 22(2):289–300.

Turkyilmaz I, Ozan O, Yilmaz B, Ersoy AE. 2008. Determination of bone quality of 372 implant recipient sites using hounsfield unit from computerized tomography: a clinical study. Clin Implant Dent Relat Res. 10(4):238–244.

Ulm C, Kneissel M, Schedle A, Solar P, Matejka M, Schneider B, Donath K. 1999. Characteristic features of trabecular bone in edentulous maxillae. Clin Oral Implants Res. 10(6):459–467.

van Amerongen R, Bowman AN, Nusse R. 2012. Developmental stage and time dictate the fate of wnt/beta-catenin-responsive stem cells in the mammary gland. Cell Stem Cell. 11(3):387–400.

Yang S, Ma K, Geng Z, Sun X, Fu X. 2015. Oriented cell division: new roles in guiding skin wound repair and regeneration. Biosci Rep. 35(6):e00280.

Yin X, Li J, Chen T, Mouraret S, Dhamdhere G, Brunski JB, Zou S, Helms JA. 2016. Rescuing failed oral implants via wnt activation. J Clin Periodontol. 43(2):180–192.